Eur. Phys. J. Plus (2021) 136:719
https://doi.org/10.1140/epjp/s13360-021-01700-9

THE EUROPEAN PHYSICAL JOURNAL PLUS

Regular Article

Toward label-free imaging of brain vasculature: frame-by-frame spatial adaptive filtration and adaptive PIV approaches

Maxim A. Kurochkin[1,2,a], **Ivan V. Fedosov**[2], **Dmitry E. Postnov**[2]

[1] Skolkovo Institute of Science and Technology, 3 Nobelya Str., Moscow, Russia 143025
[2] Saratov State University, 83 Astrakhanskaya street, Saratov, Russia 410012

Received: 26 March 2021 / Accepted: 21 June 2021

Abstract Visualization of the smallest blood vessels in the brain, capillaries, and assessment of the blood flow rate in them is important in many physiological studies. However, it is in this case that conventional label-free imaging methods fail since both the number and velocity of red blood cells in the capillaries are often too low. We present a label-free method of capillary blood flow analysis aimed at detecting and counting each single red blood cell in order to build a very detailed map of the vasculature. Such a map, in turn, enables us to more effectively apply the Particle Image Velocimetry method and make label-free blood flow velocity measurements in the smallest capillaries. Technically, our method is based on the adaptive spatial filtering of each frame of the acquired series of images using adaptive Niblack filtration. As a result of frame-by-frame filtering, we can differentiate single moving RBCs from static image artifacts having a similar size and brightness. We show the method applicability using two different biological models, specifically, the chicken embryo and the mouse brain.

1 Introduction

Recently, there has been a growing evidence that the vascular system of the brain not only performs its main function of delivering nutrients and oxygen, but also facilitate the flow of cerebral fluids and, consequently, the transport of various substances. It has been shown that perivascular spaces serve as low resistance pathways for cerebrospinal fluid flow [1]. Each of discussed scenarios for drainage of the brain parenchyma includes diving arterioles and venules as channels for cerebral fluid flow [2]. Specifically, flow through perivascular space (PVS) of arterial and venous vessels underlies the popular glymphatic hypothesis [3]. When discussing the mechanisms of this transport, an important role is assigned to pulsations of arterial vessels [4–7]. The effects of pulsations at the level of small and smallest vessels — arterioles and capillaries—are still being actively studied. It is believed that in combination with diffusion, they increase the efficiency of parenchymal drainage [8,9].

For the above reasons, it is important to be able to visualize and map velocities for the microvasculature up to the smallest vessels. When solving such problems, the methods of

[a] e-mail: maxim_optics@mail.ru (corresponding author)

Published online: 05 July 2021

fluorescence analysis are highly reliable, especially in combination with the high-resolution methods of confocal or multiphoton microscopy [10]. However, this method is expensive and requires the administration of cytotoxic dyes. Also, this method is difficult to apply when one needs to use a whole set of markers to render different objects at the same time.

For this reason, attempts to analyze the characteristics of cerebral blood flow by label-free methods persist. Label-free full-field laser speckle contrast analysis (LASCA) allows one to reconstruct the blood vessel map together with blood velocity characteristics in real-time [11]. But the spatio-temporal resolution of this technique does not allow one to analyze the smallest blood vessels because of the low concentration of scatterers red blood cells (RBC)s in the capillaries [12].

Doppler optical coherence tomography (DOCT) is also a quite expensive method for label-free vascular network 3D imaging has good enough resolution to visualize active capillary networks with a relatively high number of movement erythrocytes, otherwise, additional agents, such as intravenous intralipid administration, may be required to visualize capillaries with a low blood flow activity [13].

Let us emphasize that the greatest problems arise precisely for the smallest vessels. For large- and medium-sized vessels that are constantly filled with red blood cells, the selectivity of hemoglobin absorption allows to contrast RBCs using light sources with wavelengths that correspond to "isosbestic points" of oxy- and deoxyhemoglobin [14–16]. This method is quite simple and usually enough robust to visualize tissue surface vessels with diameters greater than 50–100 microns.

Usually, the blood flow through the capillaries is presented as the movement of red blood cells tightly enclosed to each other. However, the red blood cells move along the capillaries not only in the form of a well-observed dense flow, but also can move in the form of single RBCs, which significantly complicates the detection of the capillaries network.

The visibility of a single erythrocyte may not differ significantly from the surrounding tissue especially if observed RBCs are slightly out of focus. Further, it is impossible to guarantee that all erythrocytes will be located strongly in the focal plane of the imaging system because the blood network is not presented as parallel layers in the tissue but evenly distributed throughout the entire tissue volume.

Particle image velocimetry (PIV) is a rapidly evolving and cost effective full-field and label-free method for tracking of the moving particles. This method with sub-micron resolution is based on the calculation of correlation function of the relevant sections of a sequential pair of frames [17]. Thus, PIV is suitable for the visualization of the blood flow in the smallest capillaries.

During last two decades, Sugii et.al demonstrated in vivo the measurement of the blood velocity profile in a single blood vessel of a rat mesentery [18]. In 2007, there were attempts to analyze the cardiac activity of the chicken embryo at an early stage of development [19]. In the same year, in work Lee et al. it has been shown that accuracy of PIV method of blood measurement can be increased at the expense of a threshold filtration of fields of blood flow velocity so that velocities close to zero value during reconstruction of the velocity field were not taken into account [20]. This idea is further developed in [21,22], where it was suggested that filtered blood velocity maps characterize the spatial distribution of large blood vessels and demonstrated the ability to calculate a full field map distribution of the blood pressure and shear stress provided on the vessel walls. In 2012, it was shown that the use of fluorescent trace particles to measure blood flow via PIV does not provide significant advantages over the label-free PIV which uses blood cell as tracer particles [23].

However, the described above techniques of vascular visualization are based on the averaging of the intensity over the series of frames. Thus, these methods are not able to detect

single erythrocytes running through the capillaries. Indeed, the averaging applied to the batch of frames where only a few of them show low-intensity object (erythrocyte) inevitably leads to considerable underestimation of its intensity.

Recently, significant improvement of the PIV method was achieved using of pixel intensity cross-correlation [24]. However, the problem of visualization of the smallest capillaries has not been solved because the proposed filtration methods cannot provide the visualization of vessels with a small number of scatterers.

Poelmann et. al. in [17,22] assumed that the problems of the capillary label-free visualization can be solved by detecting vessel boundaries by the sorting of the PIV reconstructed local velocity gradient, but did not consider that PIV method application implies averaging of speed values within the calculated zones over the whole series of frames, which in its turn leads to blood flow velocity under estimations. Therefore, at the threshold filtration of blood velocity maps such a method does not allow to take into account the smallest capillaries.

In our work, we propose a method for processing the blood flow image, which ensures successful reconstruction of the morphology of the micro-circulatory network, including the smallest capillaries.

Technically, our method is based on a special application of Niblack's [25] frame by frame filtering.

Proposed algorithm is able to detect the capillaries with extremely weak blood flow, so they are rarely visited by individual erythrocytes. Using the obtained vascular map as an tree-like region of interest (ROI), we calculate the detailed map of the blood flow velocity in the smallest capillaries using the adaptive PIV analysis. We give a step-by-step description of the proposed method of data processing and demonstrate its application to the visualization of the smallest blood vessels in two different biological models, being the chorioallantoic membrane of a chick embryo, and the upper layer of the mouse brain parenchyma.

2 Materials and methods

2.1 Biological models

The chicken embryo is widely used in various hemodynamic research [26–30]. For our purpose, we use the vascular network developed in chorioallantoic membrane (CAM) of 9–11 days chicken embryo. Since in most countries, the chick embryo is not considered a live animal until day 17 of development, the CAM model we use does not require ethics committee approval for animal experiments [26,31].

When registering cerebral blood flow in a mouse, male mice (from 20 to 25 g) were housed under standard laboratory conditions, with access to food and water, ad libitum.

To access the meninges, the top of the skull was removed. After that, no additional procedures were performed, with the exception of irrigation of its surface with saline. All procedures were performed in accordance with the "Guide for the Care and Use of Laboratory Animals" [32]. The experimental protocol was approved by the Committee for the Care and Use of Laboratory Animals at Saratov State University (Protocol 7, 07.02.2018).

2.2 Imaging procedure

Visualization of vascular networks in both biological models was performed using a custom visualization setup equipped with a $10\times/0.27$ infinity corrected long work distance objective (WD = 34 mm, Nanjing KOZO CO., China), tube lens with focal distance $f = 200mm$ and

a CMOS camera (ac2040-180km, Basler Inc.). For shadow-less tissue illumination, the ring-shaped holder of 20 blue LEDs was placed on the objective case. LEDs had wavelength of $470nm$ in order to provide good RBCs contrast. Since we used a lens with a long working distance, no immersion was applied.

The grayscale 8-bit optical images of the microcirculation network were collected at the frame rate of 187 fps with size of 2040×2048 pixels, with resolution of $0.725\mu m$/pix.

2.3 Particle image velocimetry

Particle Image Velocimetry was used as a method to access the direction and velocity of blood flow within the selected regions of interest.

The pair of images with intensity distribution $f_k(i, j)$ and $g_k(i, j)$, taken at the time moments t and $t + \Delta t$, respectively, have been split into interrogation regions (IR) of size $p \times q$ pixels each. For each pair of such regions (taken from two frames), the correlation function $\Phi_k(m, n)$ has been calculated:

$$\Phi_k(m, n) = \sum_{j=1}^{q} \sum_{i=1}^{p} f_k(i, j) g_k(i + m, j + n), \tag{1}$$

where $f_k(i, j)$ and $g_k(i, j)$ are the pixels intensity of the two sequentially recorded images at a certain interrogation regions of size $p \times q$ pixels.

Next, the most probable displacement of the image portion from each IR has been calculated using the coordinates of the maximum of the correlation function in a given area. Being applied to each IR over the whole image, the above-described procedure gives a vector field of instantaneous velocity distribution averaged over the time between the consecutive images.

In this work, the IRs were located uniformly in 10-pixel steps in line with the vascular network mask so that the IRs with the centers of which did not belong to the coordinates of the calculation map of the vascular network were removed. The IR size was 40×40 pixels. A velocity map was calculated based on 30 frames or 160 milliseconds.

3 The procedure step by step

The main stages of proposed procedure are shown in Fig. 2 using the part of the vascular network image with the size of 360×360 pixels or $260 \times 260\mu m$.

Images of the vascular network were collected with a maximal rate achievable on the optical setup used, 187 frames per second with $5msec$ exposure time per frame. Then, the routine image stabilization algorithm was applied in order to minimize the interferences from embryo motion. In Fig. 1a, the portion of the recorded image is shown. Many isolated RBCs are seen, but no blood vessels are visible, since they do not fill the capillaries densely enough.

Step 1 (panel B): Time-averaging over all frames were performed:

$$I(p, q) = \frac{1}{N} \sum_{k=0}^{N-1} I_k(p, q), \tag{2}$$

where N is the number of frames in the series, k—index of frames in the raw series, p—number of pixels in the image row, q—number of pixels in the image column, $I_k(p, q)$—value of the intensity of the selected pixel, and $I(p, q)$—average value of the intensity of the pixel in the raw series of N frames, with the index of the row p and the number of the column q.

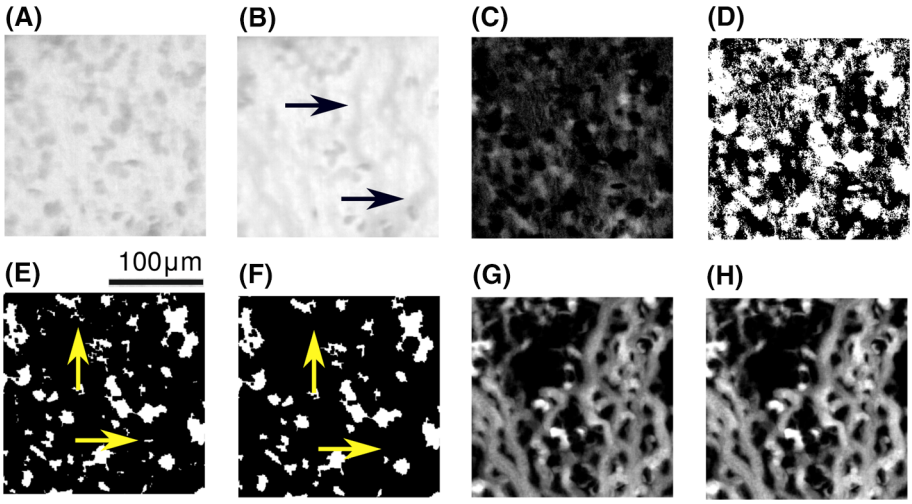

Fig. 1 The main stages of capillary blood flow label-free visualization: **a** The unprocessed optical image that contains many invisible capillaries; **b** Average intensity over the series of frames. Arrows point to poorly revealed capillaries; **c** Difference between the intensity of single frame and the average intensity of entire series; **d** adaptive Niblack threshold procedure has been applied; **e** Each frame has been two time eroded; **f** Spatial noise removal. Yellow arrows point to eliminated small artifacts; **g** Summarized intensity of cleaned from the noise images from previous step ; **h** Final image after the removal of high-frequency components via FFT analysis for the smoothing of the vessel boundaries. All images are presented in linear brightness scale for better visual perception

The result of procedure is shown in Fig. 1b. It is seen that gray tracks indicate the position of some capillaries that are more frequently visited by RBCs (pointed by black arrows).

Step 2 (panel C): In order to minimize the influence of the background, we remove all the stationary objects by subtracting the average intensity $I(p, q)$ from each frame of the series. Since the obtained images have low intensity, in Fig. 1c the representative such image is shown in 200 times increased brightness for better visual perception.

Step 3 (panel D): Adaptive image filtering using the Niblack algorithm. Each frame was divided into zones of 128 × 128 pixels, and Niblack threshold was calculated for each zone as follows [25]:

$$T(x, y) = m(x, y) + kS(x, y), \tag{3}$$

where $T(x, y)$ is a local Niblack threshold with a mean brightness magnitude $m(x, y)$ at the centered analyzed region with coordinates x and y, $S(x, y)$—standard deviation of intensity, calculated for the area of 64 × 64 pixels, $k = 0.2$—Niblack constant. The resulted binary (black and white) image is shown in panel D.

Step 4 (panel E): The erosion procedure eliminates isolated pixels and reduces the contour of bright objects to the template defined by the structuring element. For a given pixel P_0, the structuring element is centered on P_0. The pixels masked by a coefficient of the structuring element equal to 1 are then referred as P_i. In the example of a structuring element 3 × 3, the P_i can range from P_0 itself to P_8. If the value of one pixel P_i is equal to 0, then P_0 is set to 0, else P_0 is set to 1. If AND(P_i) = 1, then P_0 = 1, else P_0 = 0. The pixel value of P_i was

determined as follows:

$$\begin{pmatrix} 0 & 1 & 0 \\ 1 & 1 & 1 \\ 0 & 1 & 0 \end{pmatrix} \times \begin{pmatrix} P_1 & P_2 & P_3 \\ P_4 & P_0 & P_5 \\ P_6 & P_7 & P_8 \end{pmatrix} \rightarrow P_0 = \tau(P_0, P_2, P_4, P_5, P_7) \tag{4}$$

The processed image consists of bright patterns of different sizes which represent both the areas of the circulatory system and residual small particles which cannot be classified and should be removed.

Step 4 (panel F): Contrary to the standard erosion method, the erosion resistance test does not change object boundaries, but only removes those of them that would have been removed by a standard erosion operation. Figure 2f shows Fig. 2e processed in such a way with two consecutive erosion operations described in the previous step. The yellow arrows indicate the exemplary image elements that are eliminated by erosion resistance test method.

Step 5 (panel G): The sum of all frames processed as described above provides us the map of the small vessels that cannot be seen in the original image. However, the boundaries of the detected vessels are jagged and should be smoothed.

Step 5 (panel H): To smooth the vessel boundaries, high-frequency spatial components were filtered with 2D Fast Fourier Transform (FFT) algorithm:

$$F(u, v) = \frac{1}{NM} \sum_{x=0}^{N-1} \sum_{y=0}^{M-1} f(x, y) e^{-j2\pi(\frac{ux}{N} + \frac{vy}{M})}, \tag{5}$$

where $N \times M$ is the resolution of the spatial image $f(x, y)$, $f(x, y)$is the light intensity of the pixel with coordinates x and y. The u and v are the horizontal and vertical spatial frequencies. Then, it was performed low-pass filtering:

$$C(f) = \frac{f_{max} - f}{f_{max} - f_0} \tag{6}$$

where f_{max}—null frequency, f_{max}—maximum frequency, C —coefficient by which each frequency multiplies thus, $C(f_0) = 1$, $C(f_{max}) = 0$. Then, the inverse FFT was performed.

The result of described above operation is hardly visible by eye (see Fig. 1h) but allow a more accurate placement of interrogation regions for subsequent PIV analysis.

4 Results

4.1 Detection of small vessels

Figure 2 shows the results of applying the proposed procedure in the case of both biological models. The two panels in the upper row show an unprocessed optical image of the movement of red blood cells in the vessels of the chorioallantoic membrane of a chick embryo (panel A) and a map of the vascular network (panel B), built on the basis of processing 50 such images, which corresponds to approximately 250 ms when reading 187 frames per second.

The main obtained result is clearly visible in panel B: the detailed network has been revealed. In particular, tree-like sections (top-center area) and sections of a multi-connected network (in the center) are confidently distinguished. This difference in the type of micro-circulatory network is important in the analysis of experimental data but is completely indistinguishable in the original image in panel A.

Panels C, D, E, F in the same figure illustrate the application of the method to RBCs movement in the upper layer of the parenchyma of the mouse brain. Namely, the optical system was focused just below the level at which the "diving" of the vessels was observed from the level of the meninges into the depths of the parenchyma. This object is more difficult for analysis, since, unlike the chorioallantoic membrane of the chick embryo, the microcirculatory network does not lie within the same plane. Nevertheless, the method allows revealing a set of details of the structure of the network. We demonstrate this with four numbered fragments rendered with sub-panels on the right. The differences are clearly visible if you compare the left and right sub-panels in columns E and F.

Specifically, the sub-panels E1 and F1 show that the current optical image may not reflect the differences in the average capillary loading (marked with an arrow).

Pair E2 and F2 reveal that a capillary loop can be not visible in the original image.

Example in sub-panels E3 and F3 demonstrates an artifact—a false image of the vessel, which is present at E3, but disappeared during processing, as it does not contain moving red blood cells.

Finally, the example in E4 and F4 reveals a small vessel, almost invisible to the optical image, leaving the focal plane and having no visible continuation.

Summing up this section, the application of the proposed technique allows one to obtain more detailed information both on the structure of the microcirculatory network and on the functionality of its segments.

4.2 Velocimetry

The advanced vascular imaging technique described above allows us to apply the PIV method much more efficiently. Namely, by loading the obtained map of vessels as region of interest (ROI), computational costs can be significantly reduced. Figure 3a shows a map of capillary velocities calculated over the entire image field only for the locations where there are vessels. According to our estimates, the real savings in computer performance for this particular object were at least 8–10 times compared with the calculation for the full image field, as it would be required to apply the method for assessing the low-velocity part of the blood flow according to the method [17,22].

The second, but not the less important result, concerns the structure of the resulting network. In Fig.3b, an enlarged view of a fragment of the velocity map, the complex structure of which follows the found location of the vessels. Panels C-E show the same area, but when calculating using the method suggested in [17,22], which implies the removal of all elements that have a velocity below the selected threshold, as indicated in the figure caption. As you can see, none of these sub-panels reproduces the actual structure of the network Fig.3b.

Thus, our proposed two-stage procedure, in which the boundaries of the vascular network are first determined, and only then the PIV method is applied on the resulting mask, demonstrates an obvious advantage over the previously proposed approach.

Due to the fact that our method applies frame-by-frame filtering of the blood vessel, it became possible to analyze the movement of single red blood cells in capillaries, which was difficult using methods of blood network mapping due to threshold filtering of blood velocities obtained by standard full-frame PIV method [20-23], since standard PIV itself implies averaging over the frame series to increase analysis accuracy and consequently levels the participation of rarely running single red blood cells in the resulting blood flow maps.

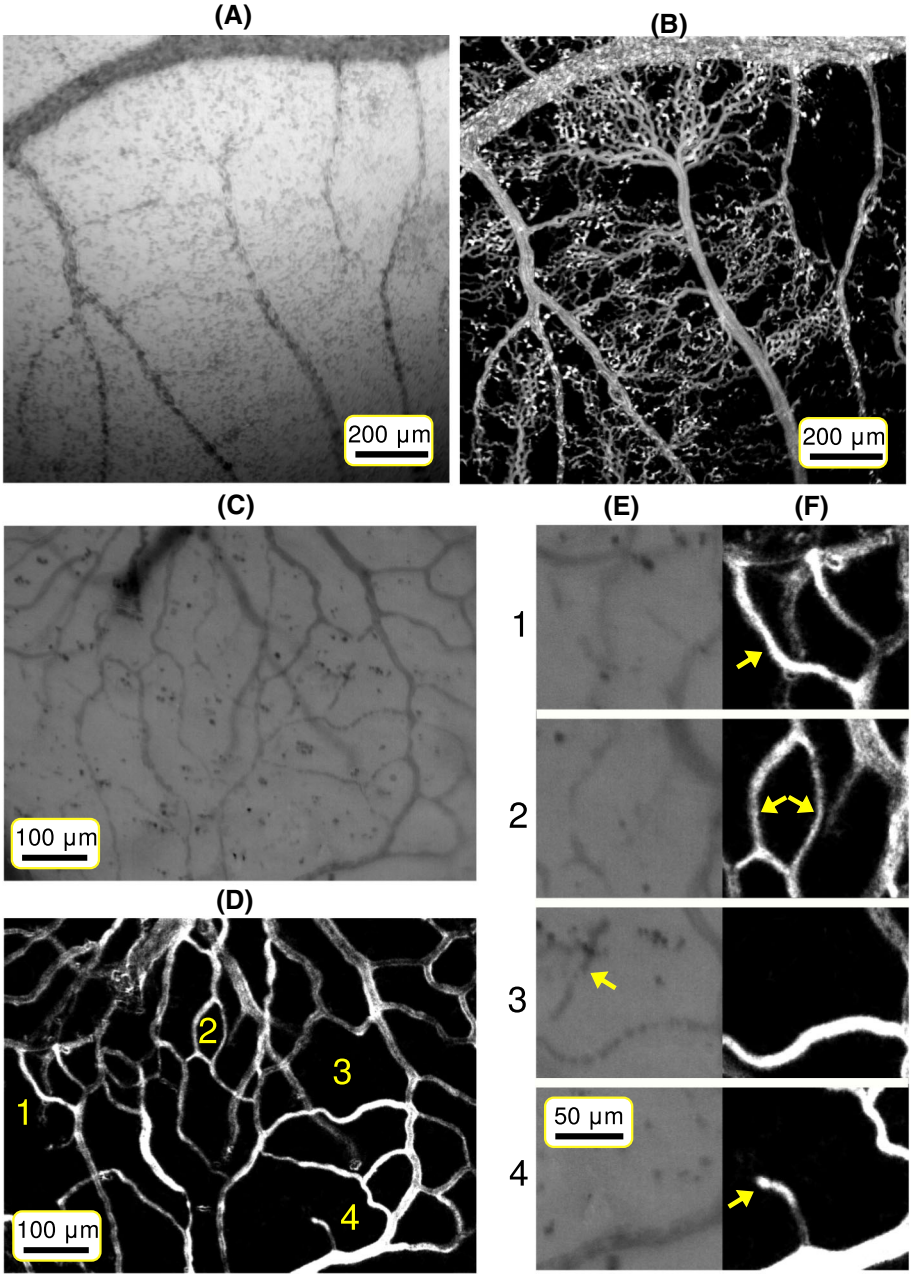

Fig. 2 Results of testing the microcirculatory network visualization algorithm. **a**, **b**: Vascular network of the chorioallantoic membrane of the chick embryo, single optical image (**a**) and the result of the proposed processing of 50 frames (**b**). **c**, **d**: The same for the upper layer of the mouse brain parenchyma. E, F: Sub-panels for comparing picture elements marked with numbers

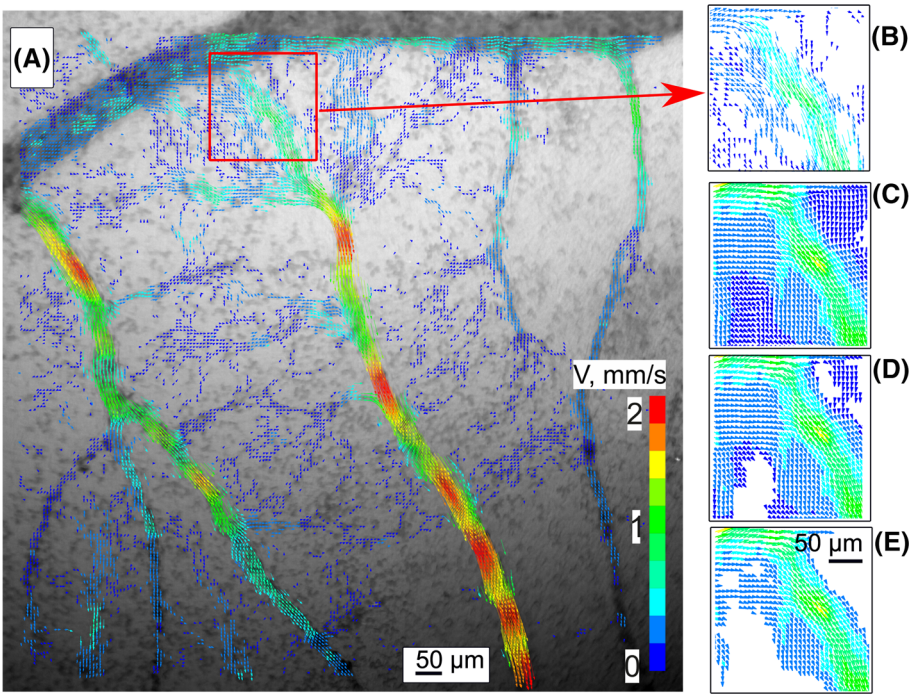

Fig. 3 PIV-powered velocity map. **a**: The vasculature map obtained in Sect. 4.1 was used as a template for calculating the velocity of RBCs. **b**: Zoomed in fragment where the structure of slow capillary flows is clearly visible. **c**–**e**: The same fragment, but with the calculation of velocities throughout all the field and subsequent removal of points where the velocity was below the threshold, being the 50-2000 $\mu m/s$, 150-2000 $\mu m/s$ and 300-2000 $\mu m/s$ for **c**,**d**,**e**, respectively

5 Conclusions

In this work, we suggested a novel cost-effective method for noninvasive vascular network full-field imaging including brain capillaries using advanced frame-by-frame adaptive spatial filtering methods based on local threshold analysis. This method allows one to reconstruct a morphological map of a branched vascular network using numeric analysis of light-field tissue images. Erythrocyte contrasting was achieved by the use of LEDs at the wavelength of the corresponding hemoglobin isosbestic point which in turn makes it possible to contrast the isolated erythrocytes using an adaptive Niblack threshold that depends on the local intensity distribution. The proposed method of frame-by-frame filtration allows one to accumulate information about individual moving erythrocytes for the reconstruction of the actual active capillary network. This method has been successfully applied to the label-free mapping of the rat brain surface. The cerebral vasculature mapping has greater cerebral vascular detail relative to unprocessed images and allows visualization of the smallest capillaries.

It should be noted, however, that further development of the method will require overcoming some problems, such as (i) too fast processes; (ii) too deeply located vessels; (iii) turbulent flows, in which erythrocytes strongly change their relative position in depth.

In the long term, we believe that the proposed approach will be useful to track the trajectory of low-contrast objects in blurred environments. This technique might also be used to analyze

the formation of blood and lymphatic vessels in the context of biomedical problems of cancer tissue vascularization or for the purpose of investigating blood vessel wall damage.

Acknowledgements This research was supported by the Russian Science Foundation, project #19-15-00201 (label-free vascular network imaging and mapping using spatial adaptive filtration, experiments on a chicken embryo) and RFBR project #19-32-60058 (M.A.K: vascular network adaptive PIV). I.V.F thanks for the support a grant from the government of the Russian Federation, project #075-15-2019-1885, in terms of the development of methods for optical imaging of brain tissue.

References

1. Beatrice Bedussi, Mitra Almasian, Judith de Vos, Ed VanBavel, Erik NTP Bakker. Paravascular spaces at the brain surface: Low resistance pathways for cerebrospinal fluid flow. J. Cerebral Blood Flow Metabol., **38**(4):719–726, 2018
2. Stephen B. Hladky, Margery A. Barrand, Mechanisms of fluid movement into, through and out of the brain: evaluation of the evidence. Fluids Barriers CNS **11**(1), 1–32 (2014)
3. Jeffrey J. Iliff, Minghuan Wang, Yonghong Liao, Benjamin A. Plogg, Weiguo Peng, Georg A. Gundersen, Helene Benveniste, G Edward Vates, Rashid Deane, Steven A. Goldman et al., A paravascular pathway facilitates csf flow through the brain parenchyma and the clearance of interstitial solutes, including amyloid β. Science translational medicine **4**(147), 147ra111-147ra111 (2012)
4. Piotr Hadaczek, Yoji Yamashita, Hanna Mirek, Laszlo Tamas, Martha C. Bohn, Charles Noble, John W. Park, Krystof Bankiewicz, The perivascular pump driven by arterial pulsation is a powerful mechanism for the distribution of therapeutic molecules within the brain. Mol. Ther. **14**(1), 69–78 (2006)
5. Jeffrey J. Iliff, Minghuan Wang, Douglas M. Zeppenfeld, Arun Venkataraman, Benjamin A. Plog, Yonghong Liao, Rashid Deane, Maiken Nedergaard, Cerebral arterial pulsation drives paravascular csf-interstitial fluid exchange in the murine brain. J. Neurosci. **33**(46), 18190–18199 (2013)
6. Alberto Avolio, Mi Ok Kim, Audrey Adji, Sumudu Gangoda, Bhargava Avadhanam, Isabella Tan, and Mark Butlin. Cerebral haemodynamics: effects of systemic arterial pulsatile function and hypertension. *Current hypertension reports*, 20(3):1–11, 2018
7. Lennart J. Geurts, Jaco JM. Zwanenburg, Catharina JM. Klijn, Peter R. Luijten, GeertJan Biessels, Higher pulsatility in cerebral perforating arteries in patients with small vessel disease related stroke, a 7t mri study. Stroke **50**(1), 62–68 (2019)
8. Mahdi Asgari, Diane De Zélicourt, Vartan Kurtcuoglu, Glymphatic solute transport does not require bulk flow. Sci. Rep. **6**(1), 1–11 (2016)
9. Ravi Teja Kedarasetti, Patrick J. Drew, Francesco Costanzo, Arterial pulsations drive oscillatory flow of csf but not directional pumping. Sci. Rep. **10**(1), 1–12) (2020)
10. Tyson N. Kim, Patrick W. Goodwill, Yeni Chen, Steven M. Conolly, Chris B. Schaffer, Dorian Liepmann, Rong A. Wang, Line-scanning particle image velocimetry: an optical approach for quantifying a wide range of blood flow speeds in live animals. PloS one **7**(6), e38590 (2012)
11. Dmitry D. Postnov, SefikEvren Erdener, Kivilcim Kilic, David A. Boas, Cardiac pulsatility mapping and vessel type identification using laser speckle contrast imaging. Biomed. Opt. Exp. **9**(12), 6388–6397 (2018)
12. S.M. Shams, Lisa M. Kazmi, Christian J. Richards, Mitchell A. Schrandt, Andrew K. Davis, Dunn, , Expanding applications, accuracy, and interpretation of laser speckle contrast imaging of cerebral blood flow. J. Cerebral Blood Flow Metabol. **35**(7), 1076–1084 (2015)
13. Jiang Zhu, Xingdao He, Zhongping Chen, Perspective: current challenges and solutions of doppler optical coherence tomography and angiography for neuroimaging. Apl. Photon. **3**(12), 120902 (2018)
14. M.A.R.Y.L. Ellsworth, R.O.L.A.N.D.N. Pittman, C.H.R.I.S.T.O.P.H.E.R.G. Ellis, Measurement of hemoglobin oxygen saturation in capillaries. Am. J. Physiol. Heart Circ. Physiol. **252**(5), H1031–H1040 (1987)
15. Roland N. Pittman, Brian R. Duling, A new method for the measurement of percent oxyhemoglobin. J. Appl. Physiol. **38**(2), 315–320 (1975)
16. Quan Liu, Tuan Vo-Dinh, Spectral filtering modulation method for estimation of hemoglobin concentration and oxygenation based on a single fluorescence emission spectrum in tissue phantoms. Med. Phys. **36**(10), 4819–4829 (2009)
17. Christian Poelma, Exploring the potential of blood flow network data. Meccanica **52**(3), 489–502 (2017)
18. Yasuhiko Sugii, Shigeru Nishio, Koji Okamoto, In vivo piv measurement of red blood cell velocity field in microvessels considering mesentery motion. Physiol. Measur. **23**(2), 403 (2002)

19. Peter Vennemann, Ralph Lindken, Jerry Westerweel, In vivo whole-field blood velocity measurement techniques. Exp. Fluids **42**(4), 495–511 (2007)
20. Jung Yeop Lee, Ho Seong Ji, Sang Joon Lee, Micro-piv measurements of blood flow in extraembryonic blood vessels of chicken embryos. Physiol. Measur. **28**(10), 1149 (2007)
21. Beerend P Hierck, Kim Van der Heiden, Christian Poelma, Jerry Westerweel, and Robert E Poelmann. Fluid shear stress and inner curvature remodeling of the embryonic heart. choosing the right lane! TheScientificWorldJOURNAL, 8, 2008
22. C. Poelma, K. Van der Heiden, B.P. Hierck, R.E. Poelmann, J. Westerweel, Measurements of the wall shear stress distribution in the outflow tract of an embryonic chicken heart. J. Royal Soc. Interf. **7**(42), 91–103 (2010)
23. Christian Poelma, Astrid Kloosterman, Beerend P. Hierck, Jerry Westerweel, Accurate blood flow measurements: Are artificial tracers necessary? PloS one **7**(9), e45247 (2012)
24. Phillip Bedggood, Andrew Metha, Mapping flow velocity in the human retinal capillary network with pixel intensity cross correlation. PloS one **14**(6), e0218918 (2019)
25. Wayne Niblack, *An Introduction to Digital Image Processing* (Prentice-Hall Inc, 1990)
26. Domenico Ribatti, The chick embryo chorioallantoic membrane (cam). A multifaceted experimental model. Mech. Dev. **141**, 70–77 (2016)
27. Patrycja Nowak-Sliwinska, M. Tatiana Segura, Luisa Iruela-Arispe, The chicken chorioallantoic membrane model in biology, medicine and bioengineering. Angiogenesis **17**(4), 779–804 (2014)
28. Laurel K. Dunn, Stephanie K. Gruenloh, Bruce E. Dunn, D Sudarshan Reddy, John R. Falck, Elizabeth R. Jacobs, Meetha Medhora, Chick chorioallantoic membrane as an in vivo model to study vasoreactivity: Characterization of development-dependent hyperemia induced by epoxyeicosatrienoic acids (eets). The anatomical record part A: discoveries in molecular, cellular, and evolutionary biology: an official publication of the American association of anatomists **285**(2), 771–780 (2005)
29. Maria Gabriella Gabrielli and Daniela Accili, The chick chorioallantoic membrane: a model of molecular, structural, and functional adaptation to transepithelial ion transport and barrier function during embryonic development. J. Biomed. Biotechnol. **2010**(2010)
30. Yong-Jie. Yuan, Xu. Kan, Wu. Wei, Qi. Luo, Yu. Jin-Lu, , Application of the chick embryo chorioallantoic membrane in neurosurgery disease. Int. J. Med. Sci. **11**(12), 1275 (2014)
31. Patrycja Tudrej, Katarzyna Aleksandra Kujawa, Alexander Jorge Cortez, Katarzyna Marta Lisowska, Characteristics of in vivo model systems for ovarian cancer studies. Diagnostics **9**(3), 120 (2019)
32. National Research Council (US). Committee for the update of the guide for the care and use of laboratory animals., institute for laboratory animal research (us), 2011